

Many-body effects on the $L_{23}VV$ Auger spectra of metals: A renormalized theory

Joseph Fitchek

*Department of Physics and Atmospheric Science, Drexel University, Philadelphia, Pennsylvania 19104
and Analytics Inc., 2500 Maryland Road, Willowgrove, Pennsylvania 19090**

Russell Patrick

Department of Physics and Atmospheric Science, Drexel University, Philadelphia, Pennsylvania 19104

Shyamalendu M. Bose

*Department of Physics and Atmospheric Science, Drexel University, Philadelphia, Pennsylvania 19104[†]
and Schlumberger-Doll Research, P. O. Box 307, Ridgefield, Connecticut 06877*

(Received 19 August 1982)

A renormalized theory has been developed to study the effects of electron-electron interaction on the line shape of the $L_{23}VV$ Auger spectrum of metals. The calculated spectrum for Al differs considerably from what would be expected for noninteracting electrons. The electron-interaction effects introduce low-energy tailing, a plasmon satellite band, and distortion of the main band.

I. INTRODUCTION

The $L_{23}VV$ Auger emission in a metal is a two-electron process in which one electron of an electron pair in the conduction band drops into a previously ionized core level and the other electron is ejected from the metal as an Auger electron. If one neglects the effects caused by the localized core hole and the interactions among the conduction electrons, the Auger line shape is proportional to the self-convolution of the conduction-band density of states,¹⁻³

$$I(2\xi - E_B) = c \int_0^{\xi_u} \rho(\xi + \Delta) \rho(\xi - \Delta) d\Delta, \quad (1)$$

where c is a constant, $2\xi - E_B$ is the energy of the ejected Auger electron, E_B being the energy of the

core state participating in the Auger process; $\xi_u = \xi$ if $\xi < E_F/2$ or $\xi_u = E_F - \xi$ if $\xi > E_F/2$ (E_F is the Fermi energy). For the noninteracting electron-gas model, the conduction-band density of states $\rho(\xi) = \alpha \xi^{1/2}$ and the calculated result is shown by the dashed curve in Fig. 1. Recent experiments by Powell⁴ and others^{5,6} on the Auger spectrum of Al, shown by the solid curve in Fig. 1, obviously disagree with the results of the free-electron model. The maximum of the experimental curve occurs at a higher energy, the main band is distorted, a low-intensity secondary peak occurs at a lower energy, and there exists a considerable amount of tailing in the low-energy region. These features indicate that electron-electron interaction effects, surface effects, energy-momentum dependence of the transition-matrix element, and the band-structure effects may play important roles in modifying the Auger line shape of Al.

In this paper we consider the effects of electron-electron interaction on the $L_{23}VV$ Auger spectra of metals. Effects of Anderson orthogonality, replacement transitions, and shake-off transitions on the position of the Auger peak have already been considered by several authors.^{7,8} In this paper we confine our attention to the role of many-body interactions on distortion of the main band, tailing, and the occurrence of the secondary peak.

Hagen and Glick⁹ calculated the plasmon satellite in the first-order effective interaction employing the techniques of the many-body perturbation theory. They used the self-energy of the electron as a

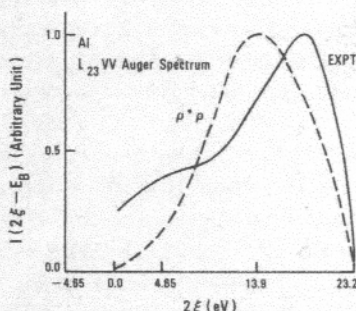


FIG. 1. $L_{23}VV$ Auger spectrum of Al. The experimental result of Powell is drawn as the solid curve. The dashed curve is obtained by self-convoluting the noninteracting electron density of states.

parameter to obtain convergence. By using a realistic value of the self-energy parameter, they found that the maximum intensity of the plasmon band is approximately 40% of that of the main band, which is larger than the experimental value. Our aim in this paper is not only to calculate the plasmon band, but also to evaluate the modification of the main band and the tailing. In order to avoid all divergence problems¹⁰ associated with such calculations, we present a renormalized theory¹¹ which includes all self-energy effects in a systematic way. The renormalization of the electron-, hole-, and core-state propagators remove all divergences, and the resulting Auger line shape develops a secondary maximum due to plasmon production and low-energy tailing and distortion of the main band due to single-particle excitations.

II. FORMULATION

The transition rate for the excitation of an Auger electron can be expressed as

$$I(\omega) \sim \sum_f |\langle \Psi_f | V_{\text{int}} | \Psi_i \rangle|^2 \delta(\omega + E_f - E_i), \quad (2)$$

where V_{int} is the Coulomb interaction responsible for the Auger transition; Ψ_i and Ψ_f are the proper solutions of the total Hamiltonian $H = H_0 + H_I$ (H_0 being the noninteracting part of the Hamiltonian and H_I being the Coulomb interaction among the electrons in the metal), with E_i and E_f as the respective eigenvalues. ω in Eq. (2) is the energy of the Auger electron and the delta function is introduced to satisfy the requirement of the conservation of energy.

Introducing an integral representation of the delta function and carrying out some minor algebra, Eq. (2) can be reduced to

$$I(\omega) = \frac{\text{Re}}{\pi} \int_0^\infty ds e^{-i\omega s} M(s), \quad (3)$$

where the correlation function $M(s)$ is given by

$$M(s) = \langle \Psi_i | O^\dagger(s) O(0) | \Psi_i \rangle \quad (4)$$

with $O^\dagger(s) = e^{iHs} V_{\text{int}} e^{-iHs}$ as the transition operator in the Heisenberg representation. Since the many-particle wave function $|\Psi_i\rangle$ for the interacting system is not known, a perturbation method is employed to construct $|\Psi_i\rangle$, which requires the use of the adiabatic theorem, S matrix, and Wick's theorem.

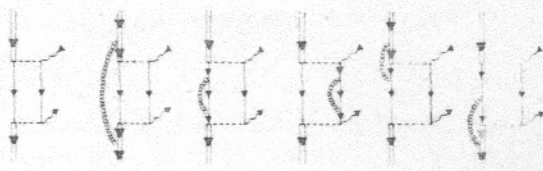


FIG. 2. Diagrams in zero and first order in effective Coulomb interaction contributing to the Auger spectra of metals.

Since we intend to use diagrammatic methods, we express $M(s)$ in the interaction representation as

$$M(s) = \langle \Phi | T \{ a_B^\dagger(\infty) O_I^\dagger(s) O_I(0) a_B(-\infty) / S \} | \Phi \rangle, \quad (5)$$

where $|\Phi\rangle$ is the initial state of the noninteracting many-particle system, T is the time-ordering operator, a_B^\dagger (a_B) is the creation (destruction) operator for the core-state electron, and S is the scattering matrix of the perturbation theory, which can be formally expressed as

$$S = T \left[\exp \left[- \int_{-\infty}^{\infty} dt H_I(t) \right] \right], \quad (6)$$

and $O_I^\dagger(s)$ is the transition potential expressed in the interaction representation as $O_I^\dagger(s) = e^{iH_0 s} V_{\text{int}}^\dagger e^{-iH_0 s}$.

The correlation function $M(s)$ now can be expressed as an infinite sum by expanding the S matrix. Each term in this expansion can be associated with a Feynman-type diagram. Typical diagrams, up to first order in effective interaction, contributing to the Auger process are shown in Fig. 2. In these diagrams the single lines pointing downward represent the holes in the conduction band. The double lines pointing downward denote the holes in the core state. The dashed lines represent the statically screened Coulomb interaction responsible for the Auger transition, and the lines of bubbles represent the effective Coulomb interaction describing the polarization of the electron gas during the Auger process. The wavy lines represent the Auger electrons.

Figure 2(a) is of zero order in effective interaction and represents the Auger process in the absence of any initial- and final-state interaction effects and is described by Eq. (1). Figure 2(b) takes into account the scattering or excitation of the conduction-band electron by the initial hole in the core state while Figs. 2(c) and 2(d) depict the polarization of the conduction band by the two final-state holes in the conduction band. Figures 2(e) and 2(f) are the interference diagrams which occur due to interference between the excitation of the conduction band by

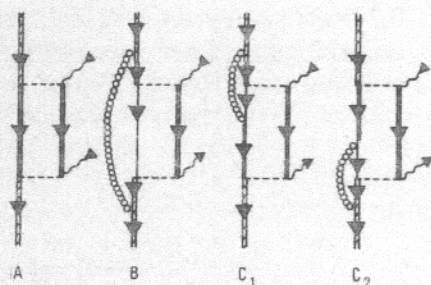


FIG. 3. Renormalized first-order diagrams contributing to the Auger process. Cross-hatched double lines are the renormalized core-hole propagators. The thick solid lines are the renormalized propagators for the electrons in the conduction band.

the core hole and that by the holes in the conduction band.

Evaluation of the first-order diagrams leads to divergence problems which have been discussed before.⁹⁻¹¹ In order to avoid such divergence problems, we have introduced a renormalization procedure which basically corresponds to replacing the bare electron-, hole-, and bound-state propagators by the corresponding renormalized propagators. This procedure leads to a renormalized first-order theory.¹¹ The renormalized first-order diagrams which have been included in our calculation are shown in Fig. 3. These diagrams contain all the diagrams of Fig. 2 and all similar higher-order diagrams. In these diagrams the cross-hatched double lines pointing downward are the renormalized core-state propagators and the thick lines pointing downward are the renormalized propagators for the holes in the conduction band. It will be noticed that some unrenormalized electron lines still appear in these diagrams. The reasons for such a procedure are discussed in detail in Ref. 11.

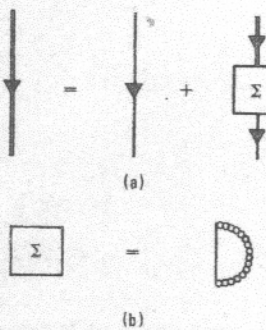


FIG. 4. (a) Diagrammatic representation of the Dyson equation satisfied by the renormalized conduction-electron propagator. (b) The self-energy is calculated in the RPA with an electron or a hole in the intermediate state.

The renormalized electron-hole propagators appearing as thick lines in Fig. 3 can be written as a Dyson equation as shown in Fig. 4(a), and can be expressed as

$$g_F(\vec{k}, \omega) = \frac{i}{\omega - \epsilon_k - \Sigma(\vec{k}, \omega)}, \quad (7)$$

where

$$\Sigma(\vec{k}, \omega) = \Sigma_1(\vec{k}, \omega) + i\Sigma_2(\vec{k}, \omega)$$

is the complex frequency and wave-number-dependent self-energy which is calculated in the random-phase approximation (RPA) [Fig. 4(b)]. The real part $\Sigma_1(\vec{k}, \omega)$ describes a shift of the bare electron energy ϵ_k and satisfies the dispersion relation

$$\Sigma_1(\vec{k}, \omega) = \Sigma_{ex}(\vec{k}) + P \int_0^\infty \frac{d\omega'}{\pi} \frac{\Sigma_2(\vec{k}, \omega')}{\omega - \omega'}, \quad (8)$$

with

$$\Sigma_{ex}(k) = -\frac{k_F \hbar^2}{\pi m a_B} \left[1 + \frac{k_F^2 - k^2}{2kk_F} \ln \left| \frac{k+k_F}{k-k_F} \right| \right], \quad (9)$$

where k_F is Fermi momentum, a_B is the Bohr radius, and $\Sigma_{ex}(k)$ is the exchange contribution calculated in the Hartree-Fock approximation.¹² The imaginary part of the self-energy describes the decay of the single-particle excitations which are not infinitely long lived due to the presence of the interactions. Calculation of this quasiparticle damping both on and off the energy shell has been carried out in the random-phase approximation by Bose *et al.*^{13,14} and others.^{15,16}

The Dyson equation satisfied by the renormalized

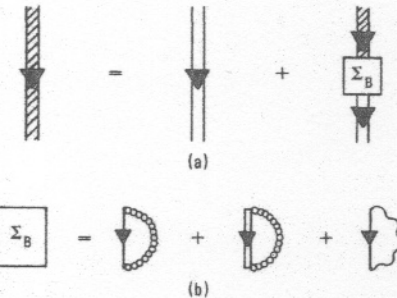


FIG. 5. (a) Diagrammatic representation of the renormalized bound-state propagator. (b) The self-energy has a radiative part and an electron interaction part with the intermediate state hole in either the core or the conduction band.

bound-state propagator is shown in Fig. 5(a) and can be written as

$$g_B(\omega) = \frac{i}{\omega - E_B - \Sigma_B(\omega)}, \quad (10)$$

where the self-energy can be expressed as

$$\Sigma_B(\omega) = \Sigma_{B1}(\omega) + i\Sigma_{B2}(\omega).$$

This self-energy of the bound-state propagator has also been calculated in the RPA [Fig. 5(b)] and has been discussed in detail elsewhere.^{11,17} For con-

sistency, the initial core-state hole will be considered along with its cloud of particle-hole pairs. Thus the observed energy E'_B of this state will include the real part of the self-energy evaluated on the energy shell

$$E'_B = E_B + \Sigma_{B1}(E_B), \quad (11)$$

and the width of this state will be taken to be

$$\Gamma_B = \Sigma_{B2}(E_B). \quad (12)$$

III. CALCULATIONS

Using the rules for calculating diagrams discussed elsewhere,¹⁰ we can write the contributions from diagrams of Fig. 3 as

$$\begin{aligned} I_A(\omega) = & -\frac{\text{Re}}{\pi(2\pi)^8} \int d\vec{p}_1 \int d\vec{p}_2 \int d\omega_1 \int d\omega_2 \int ds e^{-i\omega s} V(\vec{p}_1 - \vec{K}) V(\vec{K} - \vec{p}_1) \\ & \times \sum_{i=1}^3 f_i(\vec{K} - \vec{p}_1 - \vec{p}_2) f_i(\vec{p}_1 + \vec{p}_2 - \vec{K}) e^{-iE'_B s} \\ & \times g_F(\vec{p}_1, \omega_1) e^{i\omega_1 s} g_F(\vec{p}_2, \omega_2) e^{i\omega_2 s}, \end{aligned} \quad (13)$$

$$\begin{aligned} I_B(\omega) = & -\frac{\text{Re}}{\pi(2\pi)^{12}} \int d\vec{p}_1 \int d\vec{p}_2 \int d\vec{p}_v \int d\omega_1 \int d\omega_2 \int d\omega_v \int ds e^{-i\omega s} V(\vec{p}_1 - \vec{K}) V(\vec{K} - \vec{p}_1) \\ & \times \sum_{i=1}^3 f_i(\vec{K} - \vec{p}_1 - \vec{p}_2) f_i(\vec{p}_1 + \vec{p}_2 - \vec{K}) \\ & \times \sum_e |g_{ie}(\vec{p}_v)|^2 e^{-i(E'_B - \omega_v)s} \\ & \times g_F(\vec{p}_1, \omega_1) e^{i\omega_1 s} g_F(\vec{p}_2, \omega_2) e^{i\omega_2 s} \\ & \times g_B^2(E'_B - \omega_v) [-iV(\vec{p}_v, \omega_v)], \end{aligned} \quad (14)$$

$$\begin{aligned} I_C(\omega) = & \frac{2\text{Re}}{\pi(2\pi)^{12}} \int d\vec{p}_1 \int d\vec{p}_2 \int d\vec{p}_v \int d\omega_1 \int d\omega_2 \int d\omega_v \int ds e^{-i\omega s} V(\vec{p}_1 - \vec{K}) V(\vec{K} - \vec{p}_1) \\ & \times \sum_{i,e=1}^3 f_i(\vec{K} - \vec{p}_1 - \vec{p}_2) f_e(\vec{p}_1 + \vec{p}_2 - \vec{K}) g_{ie} \\ & \times (\vec{p}_v) e^{-i(E'_B - \omega_v)s} g_F(\vec{p}_1, \omega_1) e^{i\omega_1 s} \\ & \times g_F^0(\vec{p}_2, \omega_2) g_F(\vec{p}_2 + \vec{p}_v, \omega_2 + \omega_v) \\ & \times g_B(E'_B - \omega_v) [-iV(\vec{p}_v, \omega_v)] e^{i\omega_2 s}. \end{aligned} \quad (15)$$

Term $I_C(\omega)$ contains an extra factor of 2 since diagrams C_1 and C_2 have equal contributions. The dynamic Coulomb interaction (line of bubbles in Fig. 3) is represented by $[-iV(\vec{p}_v, \omega_v)]$, and $V(\vec{K} - \vec{p}_1)$ represents the Coulomb interaction which is responsible for the Auger transition (dashed lines in Fig. 3). The matrix element $g_{ie}(\vec{p}_v)$ occurs for the vertex in which a line of electron interaction joins an incoming and an outgoing bound-state hole and $f_i(\vec{p}_1 + \vec{p}_2 - \vec{K})$ represents the matrix element for the vertex where an interaction line joins with a core hole and a hole in the conduction band. $g_F^0(\vec{k}, \omega)$ is the noninteracting conduction electron-hole propagator. All of these quantities have been defined before.¹⁰ In addition, the renormalized conduction electron-hole propagator $g_F(\vec{k}, \omega)$ and core-state propagator $g_B(\omega)$ can be conveniently expressed in their spectral forms as

$$g_F(\vec{k}, \omega) = \int_{-\infty}^{\infty} \frac{d\omega'}{\pi} \left[\frac{i\theta(\omega' - E_F)}{\omega - \omega' + i\lambda} + \frac{i\theta(E_F - \omega')}{\omega - \omega' - i\lambda} \right] \frac{\Sigma_2(\vec{k}, \omega')}{[\omega' - \epsilon_k - \Sigma_1(\vec{k}, \omega')]^2 + \Sigma_2^2(\vec{k}, \omega')} \quad (16)$$

and

$$g_B(\omega) = \int_{-\infty}^{\infty} \frac{d\omega'}{\pi} \frac{1}{\omega - \omega' - i\lambda} \frac{\Sigma_{B2}(\omega')}{[\omega' - E_B - \Sigma_{B1}(\omega')]^2 + \Sigma_{B2}^2(\omega')} \quad (17)$$

Before proceeding to evaluate Eqs. (13)–(15), we have made several plausible approximations. First, noting that the matrix element $g_{ie}(0) = \delta_{ie}$ and that its dependence on \vec{p}_v is rather weak, we have replaced $g_{ie}(\vec{p}_v)$ in Eqs. (14) and (15) by the Kronecker delta δ_{ie} . Furthermore, all three equations contain a product of the form

$$V(\vec{p}_1 - \vec{K}) V(\vec{K} - \vec{p}_1) \sum_i f_i(\vec{K} - \vec{p}_1 - \vec{p}_2) f_i(\vec{p}_1 + \vec{p}_2 - \vec{K}), \quad (18)$$

which we have taken to be a constant α . Investigations by Hagen and Glick,^{9,17} Joyes and co-workers,^{18,19} Heine,²⁰ and Longe and Glick,¹⁰ imply that it is reasonable to neglect the momentum dependence of this expression. This expression is related to the Auger transition matrix and by setting it to a constant, we are basically assuming that the Auger transition-matrix element is energy independent.

We can now carry out the integrals over s , the frequencies and various angles in Eqs. (13)–(15). Equation (13) then takes the following form:

$$I_A(\omega) = \frac{\alpha}{(2\pi)^6} \int d\vec{p}_1 \int d\vec{p}_2 \int d\Delta \text{Im} \left[\frac{g_F(\vec{p}_1, \xi + \Delta)}{i} \right] \text{Im} \left[\frac{g_F(\vec{p}_1, \xi - \Delta)}{i} \right], \quad (19)$$

where $\xi \equiv (\omega + E'_B)/2$. This equation can be further simplified by noting that for an interacting electron gas, the conduction-band density of states is given by

$$\rho(\omega) = \frac{1}{(2\pi)^3} \int d\vec{p} \text{Im} \left[\frac{g_F(\vec{p}, \omega)}{i} \right], \quad (20)$$

so that

$$I_A(\omega) = \alpha \int d\Delta \rho(\xi + \Delta) \rho(\xi - \Delta), \quad (21)$$

which has exactly the same form as Eq. (1), except that $\rho(\epsilon)$ in Eq. (21) is the density of states of the interacting electron gas. The contribution from this diagram has been reported in previous publications.^{21,22}

We now proceed to evaluate Eqs. (14) and (15). In terms of dimensionless variables, these equations can be reduced to

$$I_B(\omega) = -\frac{6c^2\alpha}{\pi} \int \rho(\tilde{\omega}') d\tilde{\omega}' \int \rho(\tilde{\omega}'') d\tilde{\omega}'' \int dv \text{Im} \left[\frac{1}{\epsilon(v, u)} \right] \left[\text{Re} \left[\frac{g_B(\tilde{\omega}' + \tilde{\omega}'' - w2 + \tilde{E}'_B)}{i} \right] \right]^2, \quad (22)$$

$$\begin{aligned}
 I_C(\omega) = & \frac{2m^2 k_F^2 \alpha}{\pi^5} \int \frac{dv}{v} \int a da \int b db \int d\tilde{\omega}' \rho(\tilde{\omega}') \operatorname{Re} \left[\frac{g_B(\tilde{\omega}' + \tilde{\omega}'' - w2 + \tilde{E}_B')}{i} \right] \\
 & \times [\theta(0.5 - a) \operatorname{Im} V_-(v, u)] \operatorname{Re} \left[\frac{g_F(b, w2 - \tilde{\omega}')}{i} \right] \\
 & - \theta(0.25 + \tilde{\omega}' - w2) \operatorname{Im} \left[\frac{g_F(b, w2 - \tilde{\omega}')}{i} \right] [\operatorname{Re} V_-(v, 0) + \theta(a - 0.5) \operatorname{Re} V_+(v, u) \\
 & - \theta(0.5 - a) \operatorname{Re} V_-(v, u)] , \tag{23}
 \end{aligned}$$

where

$$c = \omega_p / 4E_F, \quad \tilde{\omega}' = \frac{\omega'}{4E_F}, \quad \tilde{\omega}'' = \frac{\omega''}{4E_F}, \quad w2 = \frac{\omega + E_B'}{4E_F}, \quad \tilde{E}_B' = \frac{E_B'}{4E_F},$$

$$v = \frac{p_v}{2k_F}, \quad a = p_2 / 2k_F, \quad u = \frac{w2 - \tilde{\omega} - a^2}{v}, \quad b = \frac{|\vec{p}_2 + \vec{p}_v|}{2k_F},$$

and $\epsilon(v, u)$ is the frequency and wave-number-dependent dielectric function which has been calculated in the RPA.

Calculations of I_B and I_C thus involve evaluation of three- and four-dimensional integrals over rather complicated integrand functions. In order to make these computations tractable we have made several further plausible approximations. As in the calculation of the soft-x-ray emission spectra,¹¹ we have neglected the real part of $\Sigma(\vec{k}, \omega)$ in the main band region since it does not have any important structure in this range and is not expected to alter the shape of the spectrum in any appreciable way. To avoid numerical interpolation, we have also assumed a constant value for the imaginary part of the core-state self-energy, i.e., we have chosen $\Sigma_{B2}(\omega) = \Sigma_{B2}(E_B)$ for all ω . It turns out that it is not such an unreasonable approximation in the range of ω 's in which we are interested. Furthermore, it was found that $\Sigma_{B1}(\omega)$ as calculated in Ref. 11 can be approximately fitted to a parabolic curve for values of ω of our interest. Finally, we have used the Lundqvist-Overhauser plasmon pole approximation^{23,24} in evaluating $\operatorname{Im}[1/\epsilon(v, u)]$ in Eqs. (14) and (15).

Introducing these approximations, Eqs. (13)–(15) were computed numerically for both the main band and the plasmon satellite regions for aluminum. The total contributions are plotted as the solid in Fig. 6. The dashed curve in this figure corresponds to the calculation in the noninteracting electron-gas

model. Several aspects of the calculated results are noteworthy. The electron-electron interaction effects have given rise to all the features that we were looking for. They have introduced a low-energy secondary peak due to the production of a volume plasmon during the Auger process. The electron interaction effects have also introduced a low-energy tailing of considerable strength, and a distortion of the main band due to single-particle excitations. Notice that the intensity at the secondary peak is approximately 18% of that of the main peak. The peak of the main band is only slightly shifted to the high-energy side of the spectrum.

IV. SUMMARY

In this paper we have presented a renormalized first-order theory of the $L_{23}VV$ Auger spectra of

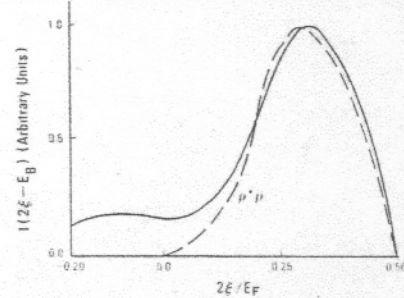


FIG. 6. $L_{23}VV$ Auger spectrum Al. The solid curve is the total intensity calculated using the renormalized theory. The dashed curve is the intensity in one-electron theory.

metals. We have considered important interaction processes which can contribute to the Auger process. We find that the renormalization of the particle and hole propagators removes the fundamental shortcomings of a first-order theory. In the renormalized theory the self-energies of the electron-, hole-, and bound-state propagators are introduced in a natural way and do not have to be treated as a parameter of the theory. As expected, our theory gives rise to tailing and distortion of the main band due to single-particle excitations and a secondary peak due to the production of a plasmon during the Auger process. The strength of the plasmon satellite is found to be approximately 18% of that of the main band, which is much higher than the ones predicted and measured in the soft-x-ray emis-

sion^{11,25} and absorption^{26,27} spectra of metals. This is in agreement with the predictions of Langreth.²⁸ Recent experiments by Baro and Tagle²⁹ show a plasmon structure of similar strength (approximately 22%) in the $L_{23}VV$ Auger spectrum of magnesium.

The first-order renormalized theory introduces only a minimal shift in the position of the Auger peak. The peak shift can be attributed partially to many-body effects^{7,8} and partially to band effects.^{30,31} The shift of the Auger peak due to the Anderson orthogonality effect, replacement transition, and shake-off transitions has already been calculated in a nonperturbative way and has been discussed in Refs. 7 and 8.

*Present address.

†Permanent address.

¹J. J. Lander, Phys. Rev. 91, 1382 (1953).

²G. F. Amelio and E. J. Schiebner, Surf. Sci. 11, 242 (1968).

³G. F. Amelio, Surf. Sci. 22, 301 (1970).

⁴C. J. Powell, Phys. Rev. Lett. 30, 1179 (1973).

⁵J. E. Houston, J. Vac. Sci. Technol. 12, 55 (1975).

⁶D. T. Quinto and W. D. Robertson, Surf. Sci. 27, 646 (1971).

⁷P. Longe and S. M. Bose, Phys. Rev. B 19, 1905 (1979).

⁸J. N. Schulman and J. D. Dow, Phys. Rev. Lett. 47, 371 (1981).

⁹A. L. Hagen and A. J. Glick, Phys. Rev. B 13, 1580 (1976).

¹⁰P. Longe and A. J. Glick, Phys. Rev. 177, 526 (1969).

¹¹S. M. Bose and A. J. Glick, Phys. Rev. B 10, 2733 (1974); S. M. Bose, Ph.D. thesis, University of Maryland, 1967 (unpublished).

¹²D. Pines, *Elementary Excitations in Solids* (Benjamin, New York, 1963), Chap. 3.

¹³S. M. Bose, A. Bardasis, A. J. Glick, D. Hone, and P. Longe, Phys. Rev. 155, 379 (1967).

¹⁴S. M. Bose and J. Fitche, Phys. Rev. B 12, 3486

(1974).

¹⁵B. I. Lundqvist, Phys. Kondens. Mater. 6, 206 (1967); 7, 117 (1968).

¹⁶L. Hedin, Phys. Rev. 139, A796 (1965).

¹⁷A. L. Hagen, Ph.D. thesis, University of Maryland, 1975 (unpublished); A. J. Glick and A. L. Hagen, Phys. Rev. B 15, 1950 (1977).

¹⁸P. Joyes and J. F. Hennequin, J. Phys. (Paris) 29, 483 (1968).

¹⁹M. Natta and P. Joyes, J. Phys. Chem. Solids 31, 447 (1970).

²⁰V. Heine, Phys. Rev. 151, 561 (1966).

²¹S. M. Bose and J. Fitche, Phys. Lett. 48A, 443 (1974).

²²J. Fitche and S. M. Bose, Phys. Lett. 54A, 460 (1975).

²³B. I. Lundqvist, Phys. Kondens. Mater. 6, 193 (1967).

²⁴A. W. Overhauser, Phys. Rev. B 3, 1888 (1971).

²⁵G. A. Rooke, Phys. Lett. 3, 234 (1963).

²⁶S. M. Bose and P. Longe, Phys. Rev. B 18, 3921 (1978).

²⁷C. Senemaud, Phys. Rev. B 18, 3929 (1978).

²⁸D. C. Langreth, Phys. Rev. Lett. 26, 1229 (1971).

²⁹A. Baro and J. A. Tagle, J. Phys. F 8, 563 (1978).

³⁰D. R. Jennison, Phys. Rev. B 18, 6865 (1978).

³¹D. R. Jennison, H. H. Madden, and D. M. Zehner, Phys. Rev. B 21, 430 (1980).